第34卷第11期 焊 接 学 报 Vol. 34 No. 11
2013年11月 TRANSACTIONS OF THE CHINA WELDING INSTITUTION November 2013

大功率激光水下切割用喷嘴设计

徐 良[1]， 王 威[1]， 李小宇[1]， 徐玉君[1]， 刘绍维[2]
(1. 机械科学研究总院 哈尔滨焊接研究所，哈尔滨 150028；2. 沈阳航天新乐有限责任公司，沈阳 110034)

徐 良

摘 要：综合考虑激光光束尺寸要求和拉瓦尔喷嘴的设计原理，对喷嘴的稳定段、收缩段、喉口及扩张段进行了设计. 稳定段尺寸主要由激光切割枪整体尺寸限制确定，收缩段连接稳定段与喉口段，采用相切圆弧过渡方式，为保证激光顺利通过喉口部位，喉口段直径大于激光光斑直径，扩张段采用直线扩张方式，鉴于切缝宽度限制，扩张角不应过大. 根据设计尺寸制造了超音速拉瓦尔喷嘴，喷出氧流速度及挺度得以改善，在激光水下切割试验中，采用局部排水法，较大氧气流量条件下顺利实现了深水条件下 30 mm 厚碳钢板的高效激光切割，与会聚型喷嘴相比，切割效果改善明显.

关键词：水下切割；激光；喷嘴
中图分类号：TG485 **文献标识码**：A **文章编号**：0253－360X(2013)11－0057－04

0 序 言

海洋资源的开发与利用是国家发展规划的重要内容之一. 海洋平台、海底管道、海底储油库等海上建筑物的建设过程、舰船建造及修复、核设施退役及核燃料解体等都离不开水下切割技术[1]. 激光水下切割技术具有切割速度快、切缝宽度窄、切割熔渣少、可进行柔性的激光传输、可进行远程控制等优点，逐渐成为国内外研究的热点[2].

研究表明[3]，激光功率一定，使用传统会聚型喷嘴进行切割时，要提高厚板的切割速度就必须提高喷嘴的供气压力. 理论研究表明，喷出气体产生激波的条件是气流压力 p_n 和周围环境的压力 p_a 之比 $p_n/p_a > 1.89$(对于双原子分子而言)时，喷出气流突然膨胀形成激波. 所以传统喷嘴在较高供气压力下喷射出的气流紊流度大，在气体流场中会产生激波，激波的存在会使得激光焦点位置发生变化，使切割面直线度下降. 涡流的存在又使熔渣排除困难，且容易导致等离子体的形成而吸收激光能量，严重影响切割质量[4-6].

根据空气动力学原理，设计一种新型拉瓦尔喷嘴，提高气体喷出速度，起到了一个“流速增大器”的作用，使得喷嘴内空气的滞压转化为动能，从而有效提高切割能力.

收稿日期：2013－05－25
基金项目：“高档数控机床与基础制造装备”科技重大专项资助项目(2011ZX04016-061)

1 超音速拉瓦尔喷嘴的设计

拉瓦尔喷嘴是一个收缩—扩张型喷管. 通过此喷头能够使具有一定压力及较低速度的气体产生超音速流. 典型的拉瓦尔喷头如图 1 所示，一般由稳定段、收缩段、喉口、扩张段 4 部分组成.

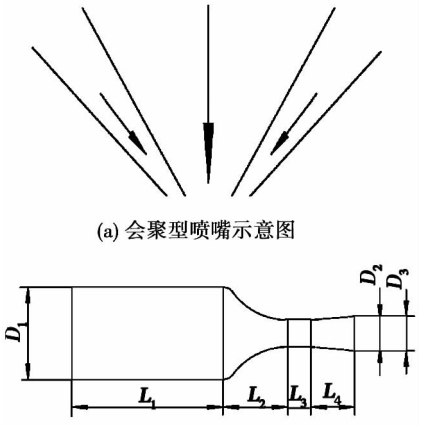

(a) 会聚型喷嘴示意图

(b) 拉瓦尔喷嘴结构

图 1 不同形式喷嘴结构示意图

Fig. 1 Different forms of nozzle structure

1.1 稳定段

稳定段的目的是使进入喷嘴的气流均匀或降低紊流度. 理论上讲稳定段直径 D_1 和喉口段直径 D_2 的直径之比越大越好，但因受与切割枪端部相连的限制，稳定段直径 $D_1 = 12$ mm. D_3 为喷嘴末端部位

直径,取3.5~4.5 mm. 稳定段长度 L_1 为喷嘴整体长度减去其它部位长度来确定.

1.2 喉口

由于喉口部位尺寸最为关键,激光光斑直径尺寸对其制约最大,直接影响到收缩段及扩张段的设计,故先进行设计.

理论上喉口部位的长度可以为0 mm,使得收缩段与喉口部位相切,但为了加工方便,喉口部位有一定长度,一般喉口长度不超过喉口直径 D_2. 喉口直径 D_2 的计算可根据以下式进行,即

$$q_m = \sqrt{\frac{K}{R}\left(\frac{2}{K+1}\right)^{\frac{K+1}{K-1}}}\frac{p_0 A}{\sqrt{T_0}} \tag{1}$$

式中: q_m 为气体流量; K 为气体的等压热容量与等容热容量之比,对于双原子分子 O_2, $K=1.4$; R 为气体常数; p_0 为气体工作压力; T_0 为气体温度; A 为喉口断面积.

由克拉伯龙方程 $pV=nRT$ 及气体物理特性可得

$$pM=\rho RT \tag{2}$$

$$q_m=\rho V \tag{3}$$

式中: p 为喷出气体压力,取 $p=0.1$ MPa; M 为氧气的相对分子量; ρ 为喷出氧气的密度; T 为喷出气体的温度; V 为气体体积.

通过式(2)和式(3),可以计算得出 q_m 约为0.5 kg/s,将 q_m 带入式(1)中,可计算得出喉口断面直径约为3.5 mm,试验过程中所用的激光最大光斑直径为2.9 mm,喉口直径为3.5 mm时激光束可顺利通过,所以取喉口部位直径 $D_1=3.5$ mm,喉口长度取3.0 mm.

1.3 收缩段

收缩段的作用是将气流从低速即小于马赫数加速到亚音速即马赫数左右. 收缩段的长度 L_2 通常取决于收缩段的半锥角、稳定段直径和喉口段直径,可按以下式计算得出,即

$$L_2=\mathrm{ctg}\alpha\left(D_1/2-D_2/2\right) \tag{4}$$

式中: α 为收缩段半锥角,取25°~30°; D_1 为稳定段直径; D_2 为喉口部位直径.

将 $D_1=12$ mm, $D_2=3.5$ mm 带入式(4),即可得出收缩段长度 $L_2=8.5$ mm.

收缩段曲线形状如图2所示,由两段圆弧相切连接构成.

根据几何关系,可以得出

$$\left(R_1+R_2\right)^2=L_2^2+\left(R_2+R_1-4.25\right)^2 \tag{5}$$

式中: R_1 为小圆弧半径,起到圆滑稳定段与收缩段的作用; R_2 为大圆弧半径,起到收缩气流,提高流速的作用; L_2 为收缩段长度.

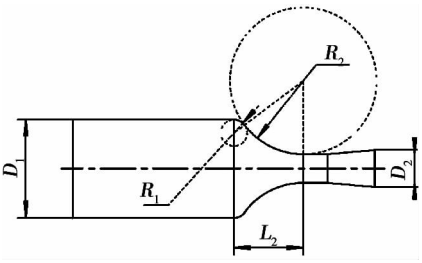

图2 收缩段结构示意图

Fig. 2 Contraction structure diagram

将 $L_2=8.5$ mm 带入式(5)中,即可得 $R_1+R_2=10.625$ mm,取 $R_1=1.625$ mm,则 $R_2=9.0$ mm.

1.4 扩张段

为了使喷嘴出口处的压力低于喉口部位的压力,并继续提高气流速度,须在喉口部位后再加一段渐扩段,这样可以在喷嘴出口处获得比音速还要大的流速即超音速,并在该处建立低压区域,此段便为扩张段.

扩张角的计算方式很多,为了简化加工流程,采用直线扩张的方式. 扩张角太大,在喷头出口处产生的激波比较严重,扩张角太小,则超音速通道很长,附面层过厚并带来压力损失. 半顶角 β 一般采用5°角. 喷嘴末端尺寸受激光光斑尺寸限制,在不影响激光输出条件下,喷嘴末端内径应不小于3.5 mm. 为了尽量减小切缝宽度,以提高激光能量利用率及减少切缝宽度,喷嘴末端内径不应大于5.0 mm,取 $D_3=4.5$ mm,根据式(6)可计算出扩张段的长度 L_4,即

$$D_3=D_2+2L_4\tan\beta \tag{6}$$

将 $D_2=3.5$ mm, $D_3=4.5$ mm, $\beta=5°$ 代入式(6)可得 $L_4=5.75$ mm.

经过以上计算,可以得出激光水下切割所使用的拉瓦尔喷嘴的尺寸如图3所示. 并根据图3所示尺寸制作了紫铜材质的喷嘴.

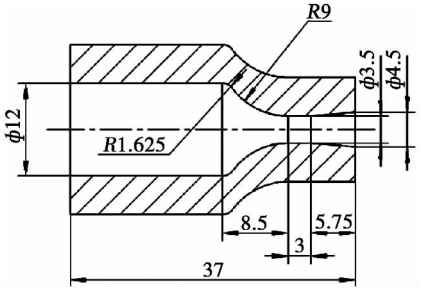

图3 激光水下切割用喷嘴(mm)

Fig. 3 Laser underwater cutting nozzle

2　水下切割试验

在特制高压水下密封试验舱内模拟深水环境,分别使用原始会聚型喷嘴和自行设计的超音速拉瓦尔喷嘴进行碳钢板激光水下切割试验.

2.1　会聚型喷嘴水下切割试验

试验参数如表 1 所示,切割效果如图 4 所示.

表 1　会聚型喷嘴水下切割试验参数

Table 1　Convergent nozzle underwater cutting test parameters

试验材料	板厚 h/mm	激光功率 P/kW	切割速度 v/(m·min^{-1})	切割氧压力 p/MPa	喷嘴直径 D/mm
Q235A	30	6.0	0.5	0.2	3.5

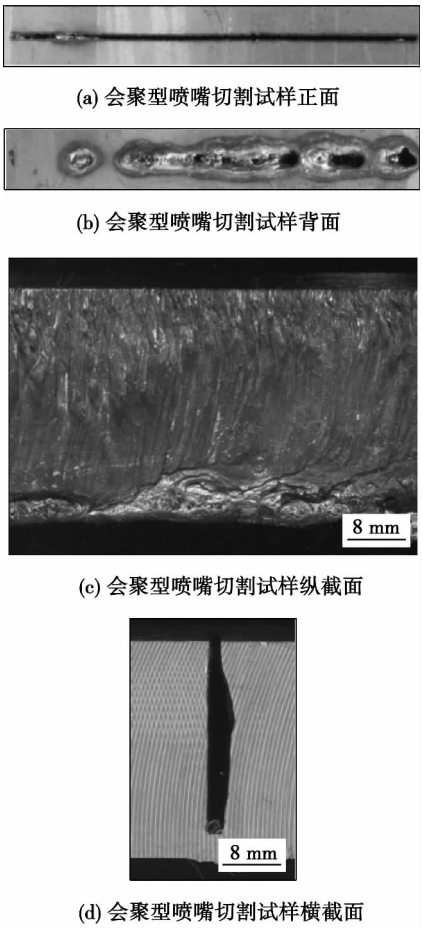

(a) 会聚型喷嘴切割试样正面

(b) 会聚型喷嘴切割试样背面

(c) 会聚型喷嘴切割试样纵截面

(d) 会聚型喷嘴切割试样横截面

图 4　会聚型喷嘴切割试验结果

Fig. 4　Convergent nozzle cutting test results

2.2　超音速拉瓦尔喷嘴水下切割试验

试验参数如表 2 所示,切割效果如图 5 所示. 经过试验可知,使用会聚型喷嘴进行水下激光切割时,在最佳切割工艺参数下,切缝难以切透,断面质量差. 当使用超音速拉瓦尔喷嘴进行切割时,切割能力明显增强,切缝质量较高,切割过程稳定,切割速度提高一倍.

表 2　拉瓦尔喷嘴水下切割试验参数

Table 2　Laval nozzle underwater cutting test parameters

试验材料	板厚 h/mm	激光功率 P/kW	切割速度 v/(m·min^{-1})	切割氧压力 p/MPa
Q235A	30	5.5	1.0	0.35

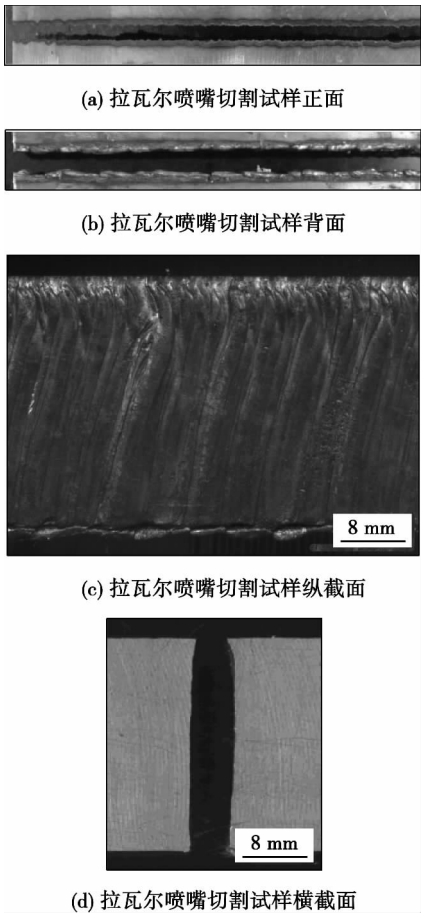

(a) 拉瓦尔喷嘴切割试样正面

(b) 拉瓦尔喷嘴切割试样背面

(c) 拉瓦尔喷嘴切割试样纵截面

(d) 拉瓦尔喷嘴切割试样横截面

图 5　拉瓦尔喷嘴切割试验结果

Fig. 5　Laval nozzle cutting test results

3　结　　论

(1) 传统汇聚型喷嘴在大气流量条件下容易产生激波,在激光水下切割厚钢板时切割效果不佳,难以直接应用.

(2) 根据激光光束尺寸特点及拉瓦尔喷嘴的设计原理,对喷嘴各部分进行了设计计算,制造了超音速拉瓦尔喷嘴.

(3) 将喷嘴应用于深水条件下激光切割试验中,采用局部排水法,顺利实现了 30 mm 厚碳钢板的高效优质切割.

参考文献:

[1] 赵寿元，李 勇，高军伟，等. 水下切割技术的研究 [J]. 机械研究与应用，2007，20(5)：26－27.
Zhao Shouyuan，Li Yong，Gao Junwei，*et al*. Research on subsea cutting technology [J]. Mechanical Research & Application，2007，20(5)：26－27.

[2] 梁桂芳. 切割技术手册 [M]. 北京：机械工业出版社，1997.

[3] 刘建华，陈一坚，段 军，等. 激光切割超音速喷嘴设计 [J]. 激光技术，2000，24(1)：47－50.
Liu Jianhua，Chen Yijian，Duan Jun，*et al*. Laser cutting supersonic nozzle design [J]. Laser Technology，2000，24(1)：47－50.

[4] 张林杰，张建勋，段爱琴. 侧吹辅助气流对激光深熔焊接光致等离子体的影响 [J]. 焊接学报，2006，27(10)：37－40.
Zhang Linjie，Zhang Jianxun，Duan Aiqin. Effect of side gas on laser induced plasma during laser deep penetration welding [J]. Transactions of the China Welding Institution，2006，27(10)：37－40.

[5] 高向东，吕威兴，游德勇，等. 大功率盘形激光焊接过程等离子体图像特征分析 [J]. 焊接学报，2011，32(12)：5－8.
Gao Xiangdong，Lü Weixing，You Deyong，*et al*. Analysis of characteristics of plasma image during high-power disk laser welding [J]. Transactions of the China Welding Institution，2011，32(12)：5－8.

[6] 崔怀洋，陈 铠，左铁钏. 适于镀锌钢板激光焊接的 CO_2 激光切割 [J]. 焊接学报，2004，25(6)：107－110.
Cui Huaiyang，Chen Kai，Zuo Tiechuan. CO_2 laser cutting for galvanized tailored welded black [J]. Transactions of the China Welding Institution，2004，25(6)：107－110.

作者简介: 徐 良，男，1984 年出生，硕士. 主要从事激光加工及复合热源焊接技术方面工作. 发表论文 7 篇. Email: xuliang9811@163.com

point of Al-Si moves to the Si side. It can be found that the phases in Al-Si-Zn brazed 6061 aluminum joint are α-Al, η-Zn, and Si particles, and the phases in Al-Si-Zn-Cu-P brazed seam are α-Al, η-Zn, fine Si particles, AlP phase.

Key words: modification; brazing; 6061 aluminum alloy; Si

Design of high power underwater laser cutting nozzle

XU Liang[1], WANG Wei[1], LI Xiaoyu[1], XU Yujun[1], LIU Shaowei[2] (1. Harbin Welding Institute, China Academy of Machinery Science and Technology, Harbin 150028, China; 2. Shenyang Xinle Aerospace Co., Ltd., Shenyang 110034, China). pp 57 - 60

Abstract: According to the principle of the laser spot size requirement and the design principle of Laval nozzle, the part of stable section, contraction section, throat section and expansion section of the nozzle were designed. The size of stable section is mainly limited by the overall size of the laser cutting gun. Contraction section is used to connect the stable period and the throat section by using tangent arc transition. In order to ensure the laser go smoothly through the throat, throat diameter must be greater than the laser spot diameter. Expansion section adopts linear expansion method, in view of the cutting seam width limit, divergence angle should not be too large. According to the design size, the supersonic Laval nozzle was manufactured, the jet velocity and stiffness of oxygen flow was improved. In underwater laser cutting experiment, using the local drainage method and larger oxygen flow, 30 mm thick carbon steel plate was cut smoothly. Compared with the convergent nozzle, the cutting effect of the supersonic nozzle has been obviously improved

Key words: underwater; cutting; laser; nozzle

Effect of rare earth Ce on microstructure and properties of Zn-22Al filler metal

WANG Bo[1], LIU Han[1], XUE Songbai[1], LI Yang[1], LOU Jiyuan[2], LOU Yinbin[2] (1. College of Materials Science and Technology, Nanjing University of Aeronautics and Astronautics, Nanjing 210016, China; 2. Zhejiang Xinrui Welding Material Co., Ltd., Shengzhou 312452, China). pp 61 - 64

Abstract: The effects of the rare earth Ce on the resistivity, melting temperature, spreadability, microstructure of Zn-22Al filler metal and shear strength of brazed joints were studied. The results indicated that the addition of Ce has little effect on the resistivity and the melting temperature of the filler metal. But with the addition of Ce, the spreadability is significantly improved, the microstructure is refined obviously. It has been found that Ce can improve the shear strength of Cu/Al joint notablely. When the content of Ce is 0.05%, the spread area of filler metal on Al and Cu substrates reached maximum values, respectively, which are 21.4% and 11.6% higher than those of Zn-22Al alloy respectively. Moreover, the shear strength of Cu/Al joint brazed with Zn-22Al-0.05Ce reaches the peak value of 91.3 MPa, which is improved by 30.3% compared with the joint brazed with Zn-22Al alloy. However, with the addition of excessive amount of Ce, some brittle Ce-bearing phases appear in the microstructure and their sizes increase, and the spreadability of filler metal and shear strength of Cu/Al joint deteriorate significantly.

Key words: rare earth Ce; Zn-Al filler metal; spreadability; microstructure; mechanical properties

Microstructure and mechanical properties of MIG welded joint of laser melting deposited TA15 titanium alloy

DU Borui, TIAN Xiangjun, WANG Huaming (School of Material Science and Engineering, Beihang University, Beijing 100191, China). pp 65 - 68

Abstract: Laser melting deposited (LMD) TA15 and rolled TA15 were welded by argon arc welding. The microstructure and phase constitution of the welded joint were studied by optical microscopy and scanning electron microscopy. The microhardness and mechanical properties of the welded joint were tested. The results indicate that the weld zone (WZ) mainly consists of columnar crystals with thick lamellar structure which epitaxially grow from the substrates. The grains in heat affected zone (HAZ) of rolled TA15 grow seriously because of its sensitivity to heat. The columnar grains in HAZ near weld zone of LMD TA15 turn into equiaxial grains. The microhardness of HAZ of LMD TA15 is the highest, while the WZ and HAZ of rolled TA15 is the lowest. The tensile strength of the welded joint is lower than that of both base metals, but the plasticity corresponds to the rolled TA15. Fracture position locates in the HAZ of rolled TA15.

Key words: titanium alloy; laser melting deposition; argon-arc welding; microstructure; mechanical properties

Fatigue life prediction of transverse cross welded joint based on different S - N curve

FAN Wenxue[1,2], CHEN Furong[1], XIE Ruijun[1], GAO Jian[1] (1. School of Materials Science and Engineering, Inner Mongolia University of Technology, Hohhot 010051, China; 2. School of Mining Institute, Inner Mongolia University of Technology, Hohhot 010051, China). pp 69 - 72

Abstract: Three kinds of S - N curves including experimental S - N curve, experience S - N curve and standard S - N curve were established by MSC. Fatigue software. The effects of residual stress, average stress and joint shape were considered. And these curves were revised according to the related criterion and used to predict the fatigue life of Q235B cross-shaped welded joint. The results show that, the fatigue damage locations of welded joint is consistent with that of experiment by S - N curve method based on MSC. Fatigue. The deviation is 7.9%-28% between the prediction values of experiment S - N curve and that of standard S - N curve. The deviation is 3.3%-19% between the prediction values of experiment S - N curve and that of experience S - N curve. The prediction values of experience S - N curve are higher than that of experiment S - N curve and that of standard S - N curve is more conservative.

Key words: cross welded joint; fatigue life; finite element analysis; S - N curve

Filler wire melting dynamics during laser beam welding with filler wire

LIU Hongbing[1], TAO Wang[2,3], CHEN Jie[1], YANG Zhibin[2], CHEN Lei[1], ZHAN Xiaohong[1], LI Liqun[2] (1.